RESEARCH ARTICLE

Reference for Electrocardiographic Imaging-Based T-Wave Alternans Estimation

ESTELA SÁNCHEZ-CARBALLO[1], **FRANCISCO MANUEL MELGAREJO-MESEGUER**[1], **RAMYA VIJAYAKUMAR**[2], **JUAN JOSÉ SÁNCHEZ-MUÑOZ**[3], **ARCADI GARCÍA-ALBEROLA**[3], **YORAM RUDY**[2], **AND JOSÉ LUIS ROJO-ÁLVAREZ**[1,4], **(Senior Member, IEEE)**

[1]Department of Signal Theory and Communications, Telematics, and Computing, Universidad Rey Juan Carlos, Fuenlabrada, 28942 Madrid, Spain
[2]Cardiac Bioelectricity and Arrhythmia Center, Washington University in St. Louis, St. Louis, MO 63130, USA
[3]Arrhythmia Unit, Hospital Clínico Universitario Virgen de la Arrixaca, El Palmar, 30120 Murcia, Spain
[4]D!lemma Ltd. Startup, Fuenlabrada, 28942 Madrid, Spain

Corresponding author: Estela Sánchez-Carballo (estela.sanchezc@urjc.es)

ABSTRACT Sudden cardiac death causes multiple deaths annually, and T-wave alternans are a reliable predictor of this fatal event. Detecting alternans is crucial for reducing disease incidence, and electrocardiographic imaging is a promising tool, providing spatial-temporal insights. The absence of references and segmentation methods specific to these data may complicate progress in the field. Therefore, this work aimed to develop a reference for evaluating estimation methods. Initially, a novel T-wave segmentation procedure specific to these data was introduced and compared with a commonly used method. Subsequently, a reference for assessing alternans estimation methods was created by integrating alternans into epicardial signals through a spatial-temporal Gaussian function. Finally, a bootstrap-based classifier for detecting alternans was developed. Results underscored the superiority of the novel T-wave segmentation procedure, with the lowest 95% confidence interval being [16.57 μV, 18.80 μV], indicating significant disparities between the two segmentation methodologies. Furthermore, the generated reference demonstrated the distinguishability of T-wave alternans with an amplitude of approximately 55 μV from noise. Additionally, the classifier exhibited consistency with previous findings, demonstrating its ability to detect alternans with amplitudes around 50 μV. In conclusion, this study provides a spatial-temporal reference for proper evaluation of estimation methods, contributing to establishing a gold standard.

INDEX TERMS Bootstrap resampling, electrocardiographic imaging, reference, spatial-temporal study, T-wave alternans, T-wave segmentation.

The associate editor coordinating the review of this manuscript and approving it for publication was Md. Kafiul Islam.

I. INTRODUCTION

Sudden cardiac death (SCD) is a concerning global issue, causing the deaths of millions of individuals and being particularly prevalent in industrialized countries [1], [2], [3]. Mitigating its incidence demands prioritized attention,

requiring a thorough examination of preventative measures. An avenue worth exploring is the identification of patients at high risk of experiencing SCD, accomplished through the utilization of SCD risk predictor indices. Several such indices exist, with heart rate turbulence indices, heart rate variability indices, and T-wave alternans (TWA) standing out as the most pertinent ones [3]. This study specifically addresses TWA, a metric quantifying beat-to-beat variations in consecutive T-wave amplitude or morphology in a surface electrocardiogram (ECG) [4]. Extensive evidence supports its accuracy in predicting malignant ventricular arrhythmia and SCD [5], [6]. It is an indicator of electrical cardiac instability, and numerous studies affirm its strong correlation with specific cardiac pathologies characterized by ventricular electrical instability, including long QT syndrome (LQTS) and Ischemic Cardiomyopathy (ICM) [7], [8], [9]. Nevertheless, TWA finds limited utilization in clinical practice. The visual identification of TWA is challenging due to the microvolt-scale variations between successive beats. Thus, a comprehensive analysis of TWA requires appropriate signal processing, estimation, and visualization techniques to attempt an effective strategy for preventing SCD [2].

A precise analysis of TWA depends on the signal processing methods employed and the availability of accurate estimation and visualization techniques. However, the lack of a definitive reference to guide the analysis process stems from the fact that no single methodology has demonstrated significant superiority over the others in this context [3]. Concerning the processing stage, two primary issues are discernible. The initial challenge involves addressing noise that coincides with the spectral range of physiological information, encompassing T waves. The removal of this noise is pivotal for accurate TWA estimation, given that slight variations in the amplitude or morphology of consecutive T-waves may share a resemblance with this in-band noise. However, removing the noise is challenging because doing so might unintentionally erase important physiological details, potentially leading to failures in TWA detection [10]. The second issue associated with the processing stage is related to the T-wave segmentation step. Inadequate segmentation of T-waves can result in the misidentification of TWA in individuals who do not actually exhibit it.

While the visual analysis of alternans is typically unfeasible, the amplitude of these alternans shows a direct correlation with heart rate [11]. As a result, healthcare professionals commonly assess the presence of TWA during exercise and ambulatory cardiac rhythm monitoring [12]. We hypothesized that TWA is regionalized in specific areas of the cardiac muscle, and for the evaluation of this hypothesis, a spatial examination of alternans is required. To achieve this, gathering not only temporal information, as conventional ECG studies do, but also spatial information becomes crucial. Non-invasive electrocardiographic imaging (ECGI) emerges as a valuable solution, providing both spatial and temporal information simultaneously [10], [13], [14]. This imaging

technique involves acquiring hundreds of simultaneous measurements of potentials at the torso level using a vest containing 256 leads, in our case. These torso signals are then merged with patient anatomical data obtained from computed tomography or magnetic resonance imaging studies. Ultimately, the inverse problem of electrocardiography is solved to non-invasively estimate epicardial signals from these measurements [14], [15], [16]. In this manner, ECGI enables a comprehensive spatial-temporal study of TWA in both the epicardium and torso. Thus far, TWA has predominantly been estimated using conventional methods, including temporal (TM), spectral (SM), and modified moving average (MMA) techniques [13]. While the TM and MMA methods estimate TWA using information in the time domain, the SM method leverages the spectral information of the signals to estimate alternans. These methods involve processing available ECG signals one by one to estimate cardiac alternans, requiring prior T-wave segmentation. These approaches are efficient when analyzing TWA in conventional ECG studies; however, due to the high quantity of ECG signals available in ECGI studies (high spatial resolution), their form of analysis becomes inefficient and time-consuming.

One of the most relevant issues associated with TWA estimation lies in the absence of a reference on which one could focus to determine the areas where TWA is present. Numerous studies prove the effectiveness of ECGI in spatially analyzing various cardiac diseases, including TWA [13], [17]. However, the lack of a definitive reference poses a challenge in confirming the accurate identification of TWA. Consequently, a reference standard capable of validating the presence or absence of TWA would be greatly beneficial. The development of such a standard would represent a significant step toward ensuring the clinical feasibility and reliability of the aforementioned TWA estimation methods. The objectives of this study were (i) to include the quantitative performance verification of a novel T-wave segmentation method first introduced in [18], (ii) to develop a spatiotemporal standard that allows the evaluation of TWA estimation methods under controlled conditions, serving as a reference for TWA analysis in real subjects, and (iii) to propose a Bootstrap-based binary classifier to ascertain the presence of TWA and, if detected, to determine its localization. The generation of the reference allowed us to perform a comprehensive analysis of available estimation methods, including their performance under noisy conditions and their accuracy in localizing cardiac areas with TWA. This helped determine which methods are more reliable and which are not. To accomplish these objectives, we used a database containing ECGI data from control subjects, ICM patients, and a LQTS patient, recorded at the Cardiac Bioelectricity and Arrhythmia Center, Yoram Rudy Lab, at Washington University in St. Louis. Using these data, we first filtered the ECG signals and segmented the T-waves with both our novel T-wave segmentation method, specifically developed for ECGI data, and one of the most commonly used T-wave

segmentation methods. We then quantitatively compared the segmentations to determine which method was superior. Next, we generated a reference by adding synthetic alternans to healthy ECG signals from a specific area of the epicardium. This allowed us to identify the exact epicardial region affected by the alternans, enabling the accurate evaluation of TWA estimation methods. The estimation methods employed in this work were the three most commonly used traditional methods, i.e., TM, SM, and MMA. By knowing the exact location and specific shape of the alternans, we could easily evaluate the performance of these methods, facilitating comparisons among them and with other methods to be developed. Finally, Bootstrap resampling was employed to detect and localize TWA. This non-parametric statistical test was defined as an intrinsic test for each subject.

This paper is organized as follows. Section II analyses significant prior works in the field. Following that, Section III presents the mathematical formulation of the problem, a concise introduction to the signal filtering and processing stages, and specifics about the reference generation process and the bootstrap resampling procedure. Subsequently, Section IV outlines the various experiments conducted. In Section V, discussions and analyses of the results are provided. Lastly, Section VI outlines the conclusions.

II. RELATED WORK

The topic of TWA has garnered significant attention and discussion since the latter half of the 20th century when the scientific community began studying its ability to predict cardiac fatal events [1]. Nowadays, this subject continues to capture the interest of numerous researchers, primarily because of its close association with SCD [19]. In recent years, considerable efforts have been dedicated to exploring TWA from a spatial-temporal perspective, exemplified by [20] and [21]. In the former, the authors presented a model of the Purkinje-ventricular system to investigate spatial-temporal abnormalities in T-waves. In the latter, the researchers focused on examining the sudden evolution of TWA into cardiac arrhythmias, underscoring the significance of spatial-temporal analysis. Spatial-temporal analyses play a key role in these instances, and ECGI holds the advantage of furnishing information in both domains. Nonetheless, there are limited studies utilizing these data to investigate TWA, with examples including [13], [22], and [23]. In [22], our group explored the presence of TWA and its spatial distribution in specific areas across the epicardium. Reference [13] exploited the spatial and temporal information provided by ECGI to examine TWA in both control subjects and patients with LQTS, yielding promising results. Meanwhile, [23] demonstrated that ECGI serves as a noninvasive approach that accurately detects the presence of TWA.

As one might surmise, accurate T-wave segmentation is imperative for estimating TWA. Various algorithms exist for T-wave segmentation, and traditionally, one prevalent method involves utilizing the position of R-waves, which

are generally the most easily detectable waves in an ECG. In [24], the Otsu method was employed to detect R-waves, and subsequently, authors utilized wavelet filters and a local maxima algorithm to segment ECG waves, achieving a 100% detection rate for R-peaks, P-peaks, and T-peaks in the utilized database. Nowadays, the incorporation of artificial intelligence (AI) is gaining prominence, with algorithms leveraging it for ECG waves segmentation. As an example, in [25], a deep learning-based model was utilized to classify ECG waves, yielding promising results. However, it was not until the publication of [18] that dedicated research elucidating a T-wave segmentation method specifically tailored for use with ECGI appeared.

Numerous studies feature computer simulations illustrating alternans, most of them employing heart models to investigate the mechanisms underlying its formation. In [26], a computational model of human ventricular cells was used to investigate the mechanisms of cardiac alternans, ultimately concluding that intracellular calcium transient alternans are the primary contributors to cardiac alternans in the human ventricle. On the other hand, in [27], authors explored alternans by simulating ECG signals with alternans, yet the specifics regarding how these simulations were conducted are not elucidated.

Given the intrinsic characteristics of TWA, defined as microvolt-sized differences between consecutive T-waves in ECG studies, its measurement is highly susceptible to interferences such as baseline noise or white noise. In [28], a time-space baseline noise cancellation method capable of minimizing noise impact without compromising the physiological characteristics of the ECG signal was devised. Another approach to mitigate various types of noise was employed in [27], where the authors leveraged AI methods to cleanse ECG signals automatically.

Lastly, using statistical methods, such as Bootstrap, to validate results or enhance existing methodologies is widespread across various research domains. In [29], a bootstrap locally interpretable model-agnostic explanation method was introduced, aiming to offer more insightful explanations for cardiac arrhythmia signal data, considering temporal dependencies between individuals. Conversely, in [30], researchers applied bootstrapping to decide on the most important variables for AI models.

After reviewing the literature, several conclusions can be drawn. Firstly, a spatial-temporal study of alternans is necessary for a complete understanding of TWA distribution. Even though ECGI is not yet broadly used, it possesses all the necessary characteristics for analyzing TWA. Due to its lack of use, there has not been any T-wave segmentation method specifically designed for ECGI data; therefore, proposing one that functions well is worthwhile. Secondly, there are few studies simulating alternans in highly controlled scenarios, and those that do often do not give it sufficient importance. This underscores the need for defining a reference that enables the identification of alternans with certainty, without relying on the assistance of a doctor who may not always

be available. Thirdly, special attention should be given to the filtering stage. Although a perfect filter does not yet exist, the use of good filters is essential when investigating TWA to avoid its confusion with noise. Fourthly, concerning the bootstrapping technique, its appropriateness for drawing inferences and serving as an alternative decision-making process has been demonstrated in the literature.

III. METHODS

In this section, the methodologies employed throughout the development of this work are detailed. Firstly, the foundational aspects of ECGI are explained. Secondly, the filtering stage is explicated. Thirdly, the T-wave segmentation methods employed in this project, namely, the atomic segmentation (AS) and single reference segmentation (SRS) methods, are outlined. Fourthly, the TM, SM, and MMA are mathematically described. Fifthly, the procedure for generating the reference is elaborated upon, and finally, the bootstrap method is explained.

ECGI involves acquiring multiple measurements of heart potentials from the body surface, facilitating a spatial-temporal analysis of the cardiac activity. Moreover, this imaging modality enables the non-invasive estimation of potentials in the epicardium by solving the inverse problem of electrocardiography. In essence, potentials are derived from the body surface, and by applying the corresponding transfer matrix, epicardial potentials can be estimated based on torso potentials. With the help of other imaging techniques, two meshes are derived – one for the epicardium and another for the torso – each featuring a distinct number of nodes. In the torso, each node represents a position where a lead was situated, and thus, potentials were measured. Conversely, in the epicardium, each node signifies the estimated potential at that specific point within the heart muscle.

Let S^2 be a two-dimensional continuous surface, representing either the epicardium or the torso, located in a three-dimensional space. Let $\mathbf{r}_{S^2}$ be the set of points in surface S^2, defined as

$$\mathbf{r}_{S^2} \equiv \{\mathbf{r} \in S^2 \mid S^2 \in \mathbb{R}^3\} \tag{1}$$

where $\mathbf{r}$ is the vector position of any point in the three-dimensional space. The potential fields, which change with time, are denoted as $\upsilon_{S^2} = \upsilon(\mathbf{r}_{S^2}, t)$. Continuous surface S^2 can be discretized, generating a geometrical mesh. In this case, for any node i belonging to the mesh, the discretized surface is defined as

$$\mathbf{s}_i = \mathbf{r}_{S^2} \cdot \delta(\mathbf{r} - \mathbf{r}_i) \tag{2}$$

where $\delta(\cdot)$ is the Dirac Delta function in the spatial domain, and the discrete set $\{\mathbf{s}_i, i = 1, 2, \ldots, N\}$ represents the N points that form the surface. Accordingly, the mesh is described as follows,

$$\mathbf{r}_{S^2}^n = \mathbf{r}_{S^2} \sum_{i=1}^{N} \delta(\mathbf{r} - \mathbf{r}_i) \tag{3}$$

Let $\Phi^{\mathbf{T}} = \{\phi_i^T, i = 1, 2, \ldots, N\}$ be the set of signals acquired on the body surface and let $\Phi^{\mathbf{E}} = \{\phi_i^E, i = 1, 2, \ldots, M\}$ be the set of estimated epicardial signals. $\mathbf{H}$ is the transfer matrix that relates $\Phi^{\mathbf{T}}$ and $\Phi^{\mathbf{E}}$ as follows,

$$\Phi^{\mathbf{T}} = \mathbf{H} \cdot \Phi^{\mathbf{E}} \quad \text{or} \quad \Phi^{\mathbf{E}} = \mathbf{H}^{-1} \cdot \Phi^{\mathbf{T}} \tag{4}$$

Regarding the filtering stage, the same filtering procedure was followed in all epicardium and torso signals. Firstly, baseline wander removal was done using a spline interpolator to remove low-frequency noise. Secondly, a low-pass filter with zero-phase distortion was used to eliminate as much high-frequency noise as possible. Therefore, the new filtered potentials could be expressed as follows,

$$\upsilon_F(\mathbf{r}_{S^2}, t) = \varpi_B(\varpi_N(\upsilon(\mathbf{r}_{S^2}, t))) \tag{5}$$

where υ_F represents the filtered potential signals, and ϖ_B and ϖ_N are the BW and high-frequency noise removal operators, respectively.

With respect to the T-wave segmentation methods, both the AS and SRS methods are compared. The former proceeds by first detecting R-waves in all the signals separately and subsequently segments T-waves based on the position of R-waves. Despite being a common method to segment T-waves, problems arise when R-waves are not adequately detected. Since ECGI data consists of hundreds or even thousands of signals, being attentive to whether all R-waves in all the signals have been properly detected is inefficient and time-consuming, making it necessary to investigate other methods that mitigate this limitation. In [18], we proposed a novel T-wave segmentation procedure, i.e., the SRS method, which leverages the synchronous activity over the entire cardiac muscle. As more detailedly explained in [18], the SRS consists of properly detecting R-waves at a single spatial point in the mesh, segmenting T-waves in that signal based on the location of R-waves, and finally, taking the starting and ending positions of the T-waves to segment them in the remaining spatial points. In this way, the SRS yields better segmentations by considering that the heart muscle functions synchronously as a unique unit.

Once T-waves are adequately segmented, TWA is estimated. For that purpose, traditional methods such as the TM, SM and MMA are used. The TM involves measuring beat-to-beat changes between even and odd T-wave amplitudes or morphology to estimate the alternan voltage V_{alt}^i as follows,

$$V_{alt}^i = T_{odd}^i - T_{even}^i \quad \forall i = 1, 2, \ldots, N \tag{6}$$

where T_{even}^i and T_{odd}^i are the even and odd T-wave templates at mesh point i, respectively, and T-wave templates were generated by averaging the corresponding T-waves at each mesh point. On the other hand, the SM estimates the power spectral density (PSD) of the temporal alternan voltage estimation V_{alt}^i as follows,

$$P^i = PSD(V_{alt}^i) \quad \forall i = 1, 2, \ldots, N; \tag{7}$$

It is obtained using the Welch overlapping segment averaging estimator and a Kaiser window. Finally, the MMA creates

T-wave templates for even and odd T-waves using the modified average instead of the sample mean, as the TM does, as follows

$$
{}_{j}^{k}T_{type}^{i} = {}_{j-1}^{k}T_{type}^{i} + \Delta \quad \forall i = 1, 2, \ldots, N
$$
$$
\forall j = 1, 2, \ldots, P; \quad \forall k = 1, 2, \ldots, K \qquad (8a)
$$
$$
T_{odd}^{i} = {}_{P}^{K}T_{odd}^{i} \quad \forall i = 1, 2, \ldots, N
$$
$$
T_{even}^{i} = {}_{P}^{K}T_{even}^{i} \quad \forall i = 1, 2, \ldots, N \qquad (8b)
$$

where P represents half of the total number of T-waves, $type = odd$ or $even$, K is the number of samples in each T-wave, and Δ is an incremental factor defined in [31]. Finally, the alternan signal V_{alt}^{i} is estimated as follows,

$$
V_{alt}^{i} = |T_{odd}^{i} - T_{even}^{i}| \quad \forall i = 1, 2, \ldots, N \qquad (9)
$$

This paper introduces a reference for the systematic evaluation of estimation methods in controlled scenarios. To achieve this objective, synthetic subjects are generated by replicating the first beat of each epicardial signal from three distinct subjects twenty times. This ensures that even and odd T-waves are identical, thus eliminating the presence of TWA. For testing TWA estimation methods, alternans are introduced at specific mesh points in a controlled manner using a spatial-temporal Gaussian function. In the spatial domain, the Gaussian is centered at a selected node, referred to as the target, and expands towards the remaining nodes based on their distance from the target. In the time domain, a Gaussian function is applied exclusively to even T-waves, with the amplitude determined by the distance of each node from the spatial Gaussian center. These synthetic subjects can serve as examples where the location of TWA is precisely known, facilitating the comparison of different estimation methods under controlled scenarios. This ensures when they perform adequately and when they do not. Synthetic alternans were incorporated into epicardial signals, while torso signals were estimated by solving the direct problem of cardiology by applying the transfer matrix.

Finally, bootstrap is employed to statistically assess the obtained results and make a decision regarding the presence of TWA. Bootstrapping involves artificially sampling the available dataset with replacement, generating new repeated samples. While this approach does not offer new information about the population, it allows for quantifying the sampling variability, enabling inferences based on the available data. To statistically assess the results, bootstrap resampling is applied patient-wise to facilitate the extraction of inferences. One of the primary advantages of this technique is its ability to derive confidence intervals (CIs) without requiring additional sampled data. In this context, a hypothesis test is formulated to determine whether the differences between the AS or SRS segmentations are significant or not. On the other hand, to decide whether there is TWA in specific points in the mesh, bootstrap is applied differently. Consecutive even and odd T-waves are subtracted from each other, and

TABLE 1. ECG signals duration, T-waves duration, and the number of beats in ECG signals for all subjects in our dataset, including control subjects (C1 - C3), ICM patients (ICM1 - ICM7), the LQTS patient (LQTS), and synthetic patients (SS1 - SS3). The units for duration measurements are in seconds.

	Signal Duration	T-Wave Duration	Number of Beats
C1	65.38	0.26	65
C2	36.00	0.25	29
C3	34.00	0.20	33
ICM1	9.26	0.23	9
ICM2	5.59	0.28	5
ICM3	9.59	0.20	14
ICM4	10.49	0.33	10
ICM5	69.48	0.16	128
ICM6	9.76	0.30	8
ICM7	9.76	0.22	10
LQTS	60.00	0.35	57
SS1	21.48	0.26	20
SS2	24.41	0.25	20
SS3	10.74	0.22	20

in each bootstrap step, the order of T-waves changes—meaning that T-waves are sampled with replacement. Using the Bonferroni correction, a CI is then derived for each mesh node, and original values are checked to determine whether they lie inside or outside the corresponding CI. If they are outside, it indicates that the order matters, signifying that the differences between even and odd T-waves are significant. Otherwise, it is assumed that the order does not affect.

IV. EXPERIMENTS

In this section, we present the experiments that have been carried out during the development of this work. First, we compare the AS and SRS methods to support the findings discovered through the visualizations in [18] and to justify the use of the SRS method moving forward. After that, we assess the behavior of our reference, and finally, we propose a statistically based way of determining the presence of alternans and demonstrate its potential using the reference. The ECGI database used in this work consists of recordings from three control subjects, seven patients with ICM, and one patient with LQTS. All the data were acquired at the Cardiac Bioelectricity and Arrhythmia Center, Yoram Rudy Lab at Washington University in St. Louis, as part of previous studies [32], [33]. Torso measurements were extracted using body surface potential mapping, and epicardial potentials were estimated by solving the inverse problem in cardiology [14]. Transfer matrices for estimating torso potentials from epicardial signals were available for two control subjects and one ICM patient. The data do not contain further information but only include the subjects ECGI measurements. All subjects signed the corresponding informed consent, and the protocols were reviewed and approved by the Human Research Protection Office at Washington University in St. Louis. The data were acquired under NIH–NHLBI grant numbers R01-HL033343 and R01-HL-049054, awarded to Prof. Yoram Rudy. Table 1 shows a
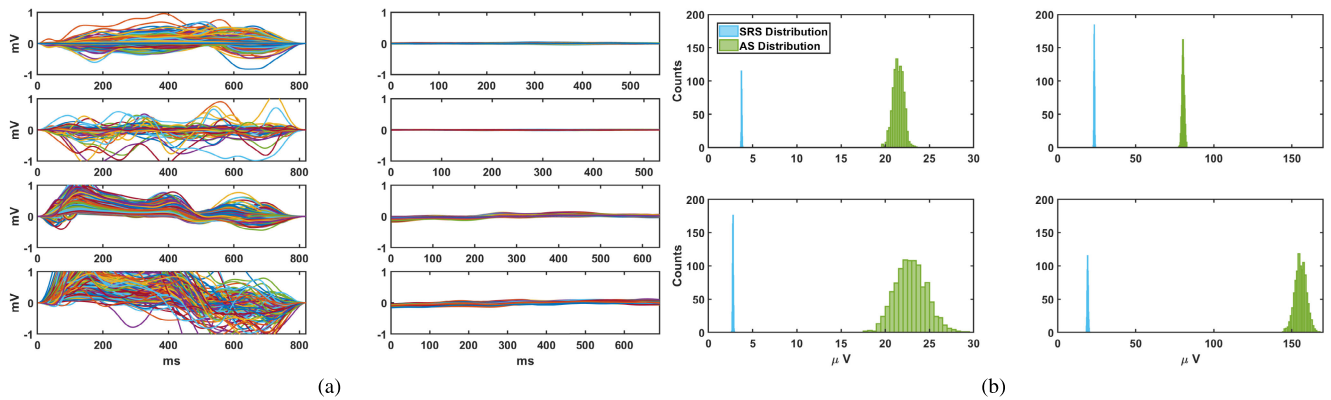
FIGURE 1. Comparative analysis of T-wave segmentation methods. (a) Differences between epicardial (odd rows) and torso (even rows), with even and odd T-waves segmented using the AS (left) and SRS (right) methods for a control subject (top two rows) and an ICM patient (bottom two rows). (b) Histograms depicting the distribution of differences between even and odd T-waves from epicardial (top row) and torso (bottom row) signals, for the controls group (left) and patients group (right), obtained using the bootstrapping technique.

TABLE 2. Empirical statistics (mean ± standard deviation) and 95% CIs in control subjects (A) and patients with ICM (B). The asterisk denotes significance. Units of measurement are μV.

(A) Results in Control Subjects

	AS empirical statistic	SRS empirical statistic	Empirical differential statistic	95% confidence interval
Epicardium	21.45 ± 10.17	3.75 ± 0.75	17.70 ± 9.42	[16.57, 18.80]*
Torso	23.02 ± 14.32	2.78 ± 1.26	20.25 ± 13.06	[16.74, 23.70]*

(B) Results in Patients

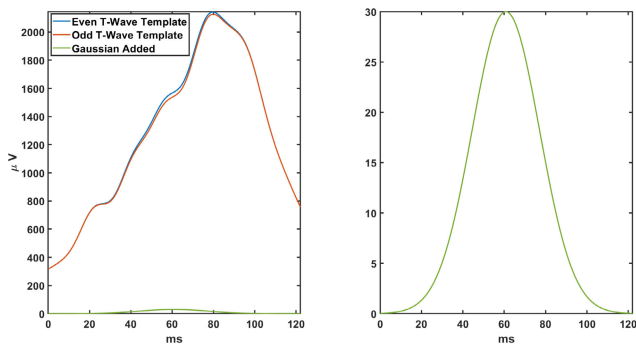|	AS empirical statistic	SRS empirical statistic	Empirical differential statistic	95% confidence interval
Epicardium	80.34 ± 44.61	23.49 ± 11.38	56.85 ± 33.24	[55.20, 58.65]*
Torso	155.41 ± 130.60	19.22 ± 13.19	136.18 ± 117.42	[129.10, 143.46]*

FIGURE 2. Even and odd T-wave templates at a mesh point in a synthetic patient along with the modifying gaussian-shaped curve (left), and an enlarged view of the added gaussian modulation (right).

summary of the characteristics of the ECG signals used in this work.

A. COMPARISON OF THE AS AND SRS METHODS
Two T-wave segmentation approaches are compared in this subsection, i.e., the AS and the SRS methods. For that purpose, T-waves were segmented using both methodologies and results were statistically assessed using a bootstrap resampling scheme applied patient-wise. Control subjects

were analyzed separately from ICM patients, and epicardium and torso signals were also independently analyzed. In this scenario, two groups of T-waves were generated, i.e., the one in which the AS method was used and the group in which the SRS method was employed. For each group, even and odd T-waves were subtracted, giving rise to signals $Ss_i^m \; \forall i = 1, 2, \ldots, R$, where R is the number of patients belonging to the groups and m is the T-wave segmentation procedure. The standard deviation of each of these signals was calculated, and afterward, the mean of the standard deviations in each group was computed as follows,

$$\overline{\sigma^m} = \frac{1}{R} \sum_i^R std(Ss_i^m) \tag{10}$$

Finally, the following hypothesis test was addressed:

$$\begin{cases} H_0 : \overline{\sigma^{AS}} - \overline{\sigma^{SRS}} = 0 \\ H_1 : \overline{\sigma^{AS}} - \overline{\sigma^{SRS}} > 0 \end{cases} \tag{11}$$

Figure 1 (a) shows the differences between consecutive even and odd T-waves segmented with the AS and SRS methods on the left and right, respectively. Qualitatively, it is evident that the SRS method provides better-quality segmentations, reducing the presence of noise, as previously reported in [18]. Quantitatively, this is also supported by
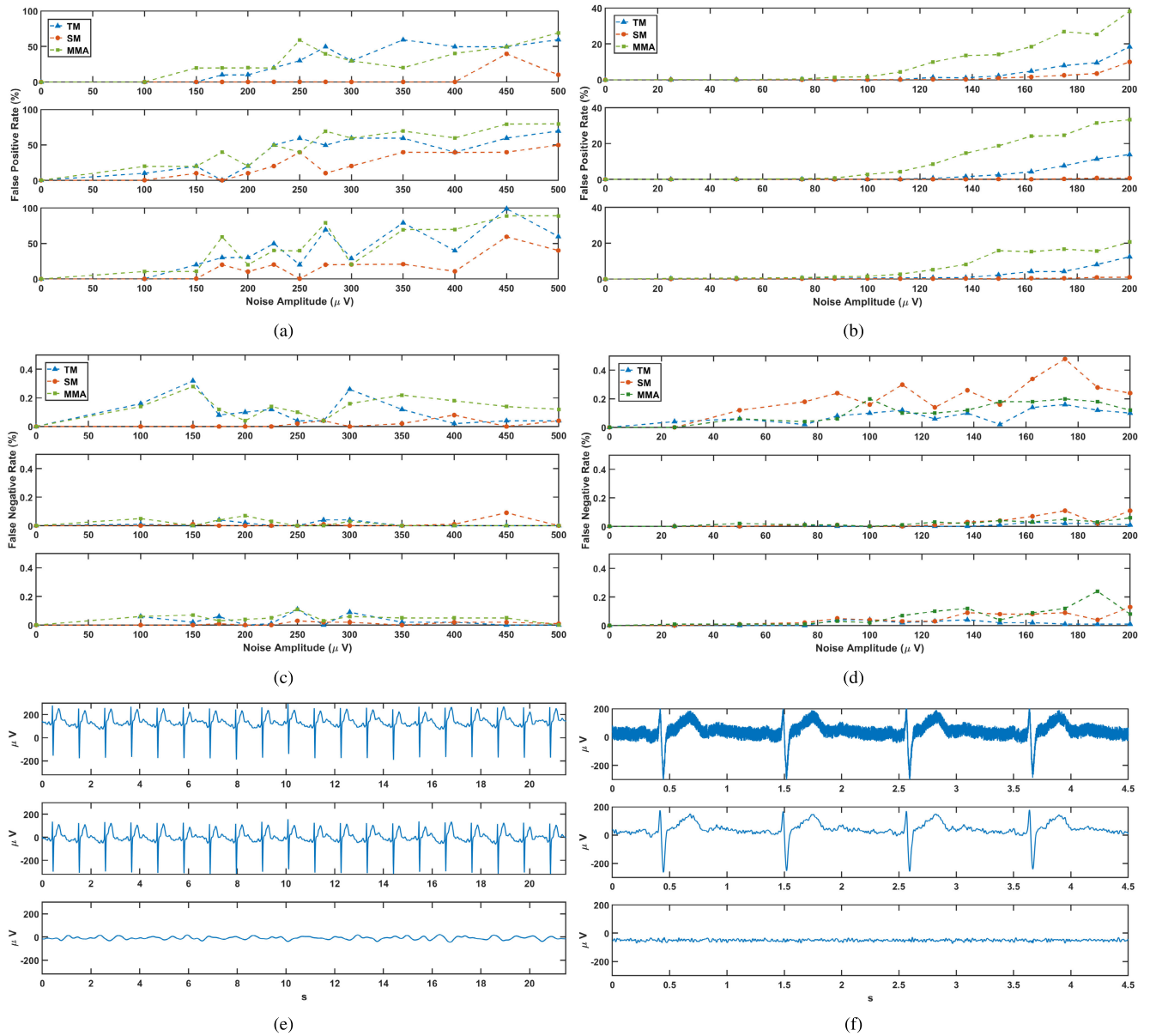
FIGURE 3. Analyses of false positive and false negative rates for increasing baseline and white noise amplitudes in synthetic patients. (a-b) False positive rates with increasing amplitudes of baseline (a) and white (b) noise for synthetic patients 1 (top), 2 (middle), and 3 (bottom). (c-d) False negative rates with rising baseline (c) and white (d) noise amplitudes for synthetic patients 1 (top), 2 (middle), and 3 (bottom). (e-f) ECG signals at an epicardium mesh point affected by baseline (e) and white (f) noise (top), showcasing the filtering process (middle) and the residuals generated by subtracting the original signal from the filtered one (bottom).

results in Table 2, where the CIs in the last column indicate the veracity of the alternative hypothesis for both epicardium and torso signals in control subjects and ICM patients. This can also be visualized in Figure 1 (b), where the AS and SRS distributions generated after applying the bootstrapping technique are included. In all cases, the distributions are clearly separated from each other, and the SRS distribution is always closest to zero, being below $5\mu V$ in control subjects and around $20\mu V$ in patients, whereas the AS distribution is above $20\mu V$ in control subjects and surpasses $150\mu V$ in patients torsos.

B. ASSESSMENT OF THE REFERENCE

In this subsection, the reference is evaluated through different experiments. Three synthetic subjects were created and used to form the reference. Synthetic signals were generated using real subjects for whom the transfer matrices were available, namely, one ICM patient and two control subjects. Alternans was synthetically incorporated into epicardial signals as detailed in Section III, with a maximum amplitude of $30\mu V$ in the target even T-waves. Figure 2 displays the temporal Gaussian-shaped function in green, along with the odd T-wave template in red and
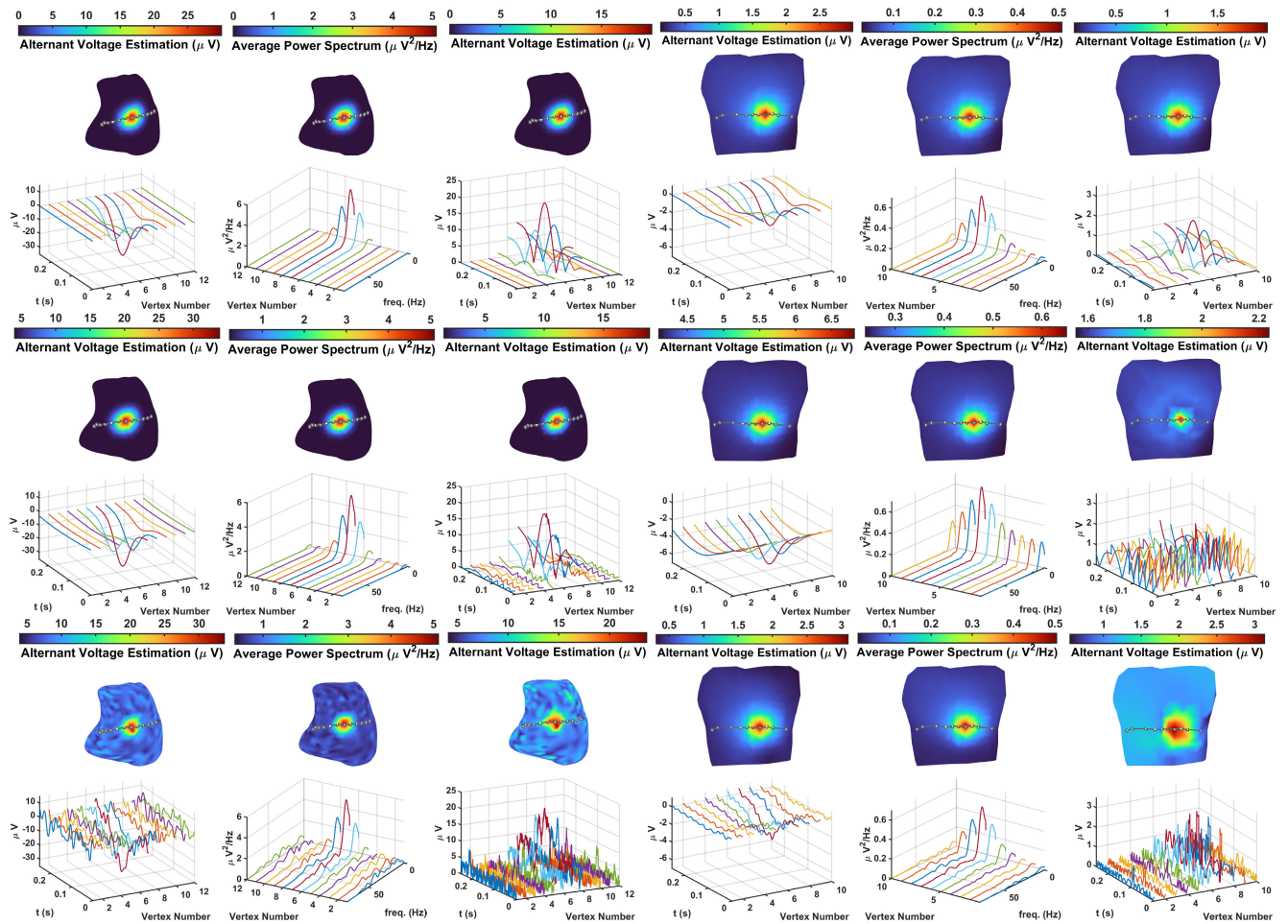
FIGURE 4. TWA maps and corresponding TWA signals at various points surrounding a target point, estimated by the TM, SM, and MMA in the epicardium and torso of a synthetic patient. Rows depict scenarios with no noise (top), baseline noise (middle), and white noise (bottom), while columns correspond to TM (first and fourth), SM (second and fifth), and MMA (third and sixth) TWA estimations. Mesh colors represent the maximum absolute value of the estimated TWA signal.

the slightly modified even T-wave template in blue at the target.

First, the focus was put on the filtering stage. Initially, baseline noise with different amplitudes was added to epicardial signals, which were then correspondingly filtered out. Independently, the same process was repeated with white noise. After that, TWA was estimated with the TM, SM, and MMA. For each signal in the mesh, the estimation methods provided a value corresponding to the maximum TWA, i.e., $TWA_{max}^i \ \forall i = 1, 2, \ldots, N$, where N is the number of nodes in the mesh, and the threshold to determine the presence of TWA was set to be $th = \frac{TWA_{max}^j}{2}$, where j is the node in which TWA_{max} was the maximum. In this way, a false positive case was one in which synthetic alternans was not added, but the estimation methods detected TWA, and a false negative case was one in which synthetic alternans was added, but the estimation methods detected that TWA was not present.

Figure 3 (a) and (b) show the percentage of false positive cases as the baseline and Gaussian noise amplitude increase, respectively. Figures 3 (c) and (d) show the percentage of

false negative cases as the baseline and Gaussian noise amplitude increase, respectively. The results consist of an average of the ten repetitions that have been carried out to increase their reliability. In general, as the noise amplitude increases, the false positive rate increases, which is always true when adding white noise. The behavior in the three synthetic patients seems to be similar. Regarding the three estimation methods, it can be observed that the SM (red) tends to be more stable than the TM (blue) and the MMA (green), which seems to perform the worst, especially when white noise is added. It can also be seen that the percentage of false negatives does not surpass 0.5%, which is significantly smaller than the false positive rate for the two types of noise. Figure 3 (e) and (f) display a signal in the epicardium of a synthetic subject to which $175 \mu V$ of baseline and $200 \mu V$ of white noise amplitude have been added, respectively. The last row, which shows the subtraction between the original signal and the filtered signal displayed in the second row, indicates that any of the filters eliminate physiological information, but some of the distortions introduced by the
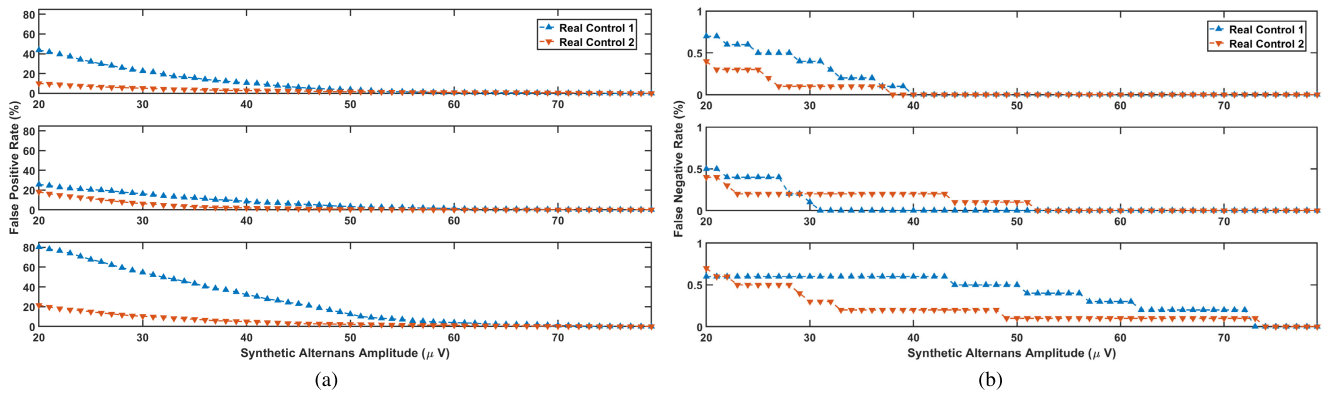
FIGURE 5. Impact of synthetic alternans amplitude on TWA estimations in real control subjects. False positive (a) and negative (b) rates with varying amplitudes of synthetic alternans added, illustrating TWA estimation by TM (top), SM (middle), and MMA (bottom).
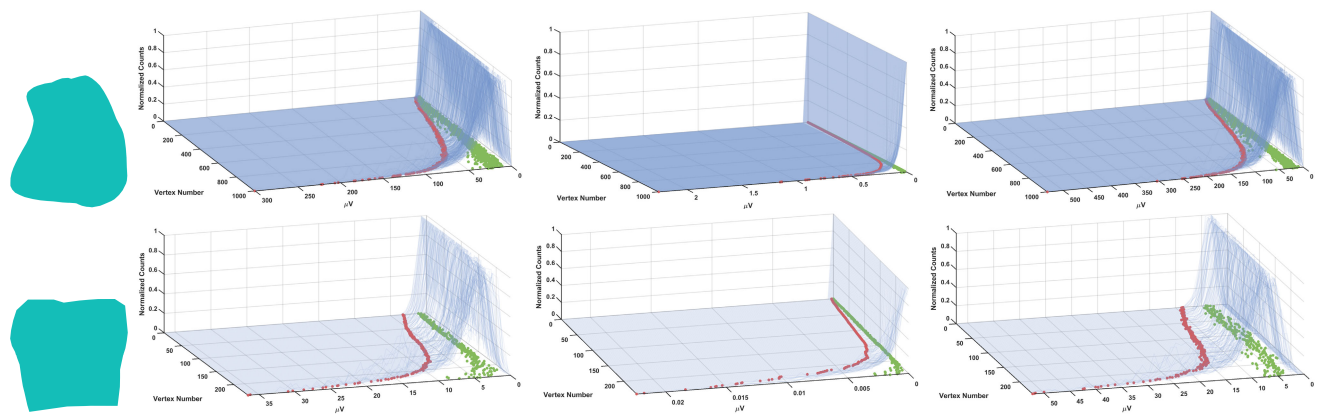

FIGURE 6. TWA maps (left) and histograms of the distribution of TWA in a control subject epicardium (top) and torso (bottom), with TWA estimated by the TM (second column), SM (third column), and MMA (right). Red circles denote CI right limits, while green circles represent empirical values for each mesh point, and mesh color indicates conformity of empirical values with their respective CIs.

noises remain since they have not been properly eliminated. Note that before applying any filter, the original signal mean is subtracted to center the signal around zero, thus improving the performance of subsequent filters.

Figure 4 illustrates the meshes and the TWA signals at points near the target in one of the synthetic subjects. Synthetic alternans were added to epicardial signals, while torso signals were obtained by applying the transfer matrices, and TWA signals were estimated with the TM (first and fourth columns), SM (second and fifth columns), and MMA (third and last columns). It should be noted that the results in the other two synthetic subjects are qualitatively equal, so only one subject was chosen to be shown. In the first row, no noise was added to the signals, so it can be observed that the three estimation methods provide a clean TWA estimation around the target. The second row shows the results when $175\mu V$ of baseline noise amplitude has been added to the signals and correspondingly filtered. In this case, we can see that estimations are clearly noisier, and the MMA torso TWA estimation has deteriorated. In the last row, the results when $200\mu V$ of white noise amplitude has been added to the signals and correspondingly filtered are displayed. As in the previous

case, noisier estimations are obtained, especially with the MMA method. In general, it seems that SM TWA estimations are more consistent over the three scenarios, and MMA TWA estimations are the noisiest and of the worst quality.

After analyzing the estimation of alternans under noisy conditions in the reference models, an analysis of real subjects was performed. Synthetic alternans was added to epicardial signals from control subjects in the same way that it was added to the reference. Figure 5 displays the percentage of false positive (a) and negative (b) cases as the maximum amplitude of the added alternans rises when TWA has been estimated with the TM (top), SM (middle), and MMA (bottom). The SM seems to be the most stable and capable of recognizing the area where alternans was added, and the percentage in the MMA is the highest, indicating that it struggles to recognize the area with TWA. Figure 5 suggests that adding $55\mu V$ of alternans is enough for the estimation methods to characterize the area with TWA, except for the MMA, which needs more than $70\mu V$ not to produce false negative cases. Our results regarding the performance of different TWA estimation methods align with those in the literature. While the MMA has been demonstrated to be more
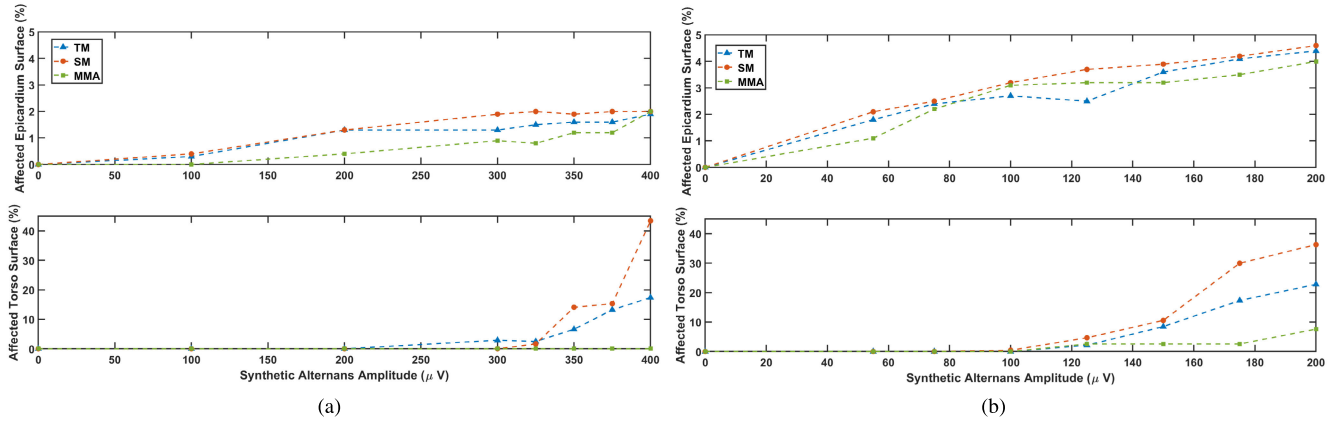
FIGURE 7. Affected epicardium (top) and torso (bottom) surfaces as the amplitude of synthetic alternans increases in control subject 1 (a) and 2 (b).
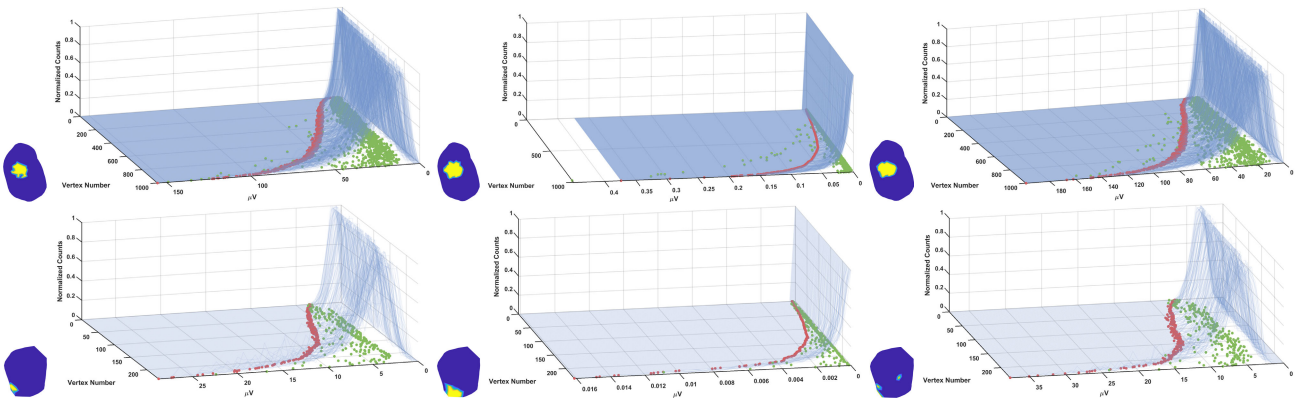

FIGURE 8. Epicardium (top) and torso (bottom) TWA maps (odd columns) and histograms of the distribution of TWA (even columns) in a real control subject with $125\mu V$ synthetic alternans amplitude added, with TWA estimated by TM (left), SM (middle), and MMA (right). Red circles denote CI right limits, green circles represent empirical values, and mesh color indicates whether empirical values are inside (blue) or outside (yellow) the CIs.

accurate in analyzing Holter studies, particularly with longer signals [12], [31], the SM, which assumes the stationarity of the ECG signal, has been reported as more accurate in conventional ECG studies and is sometimes considered the best approach in these contexts [13], [19]. Additionally, some studies highlight the efficiency of the TM despite its simplicity [5], [13], [22]. This explains why the SM appears to outperform the other estimation methods, specifically the MMA.

C. STATISTICAL METHOD TO ESTIMATE TWA

Even though traditional TWA estimation methods have been proven to perform well under different scenarios, there are some cases in which their performance could improve. In this section, we propose a new statistical TWA estimation method based on the bootstrapping methodology to boost the performance of traditional approaches. In this new approach, TWA is estimated with the TM, SM, or MMA, and the statistic s_i is computed as the mean of the standard deviation of these differences, i.e., $\hat{s}_i^j = \overline{\sigma_{even-odd}} \ \forall i = 1, 2, \dots, N$ and $\forall j = 1, 2, \dots, b$. At every bootstrapping step, the order of T-waves changes until the process is repeated b times for

the N nodes belonging to the mesh. This process facilitates the extraction of CIs, which are used to determine whether TWA exists or not, as follows,

$$\begin{cases} TWA = 0 & \text{if} \quad s_i \in CI_i \quad \forall i = 1, 2, \dots, N \\ TWA = 1 & \text{if} \quad s_i \notin CI_i \quad \forall i = 1, 2, \dots, N \end{cases}$$

With this new method, no TWA was encountered in control subjects, and it marked as positive the area where alternans were added in the reference. Figure 6 illustrates the results of this method in one of the control subjects. The histograms represent the times (z-axis) that $\hat{s}_i$ equals a specific quantity of microvolts (x-axis) in all the nodes $i = 1, 2, \dots, N$ (y-axis) during the bootstrap procedure, for TM (second column), SM (third column), and MMA (last column) estimates. Red circles indicate the right limit of the CI for each node, and it can be seen that all $\hat{s}_i$, drawn as green circles, are located to the right of the red circles, indicating that TWA does not exist. Comparing the three estimation methods through the histograms in Fig. 6, it can be observed that $\hat{s}_i$ is significantly smaller in the SM than in the other methods, being the highest in the MMA, but not too far from the TM. This supports the
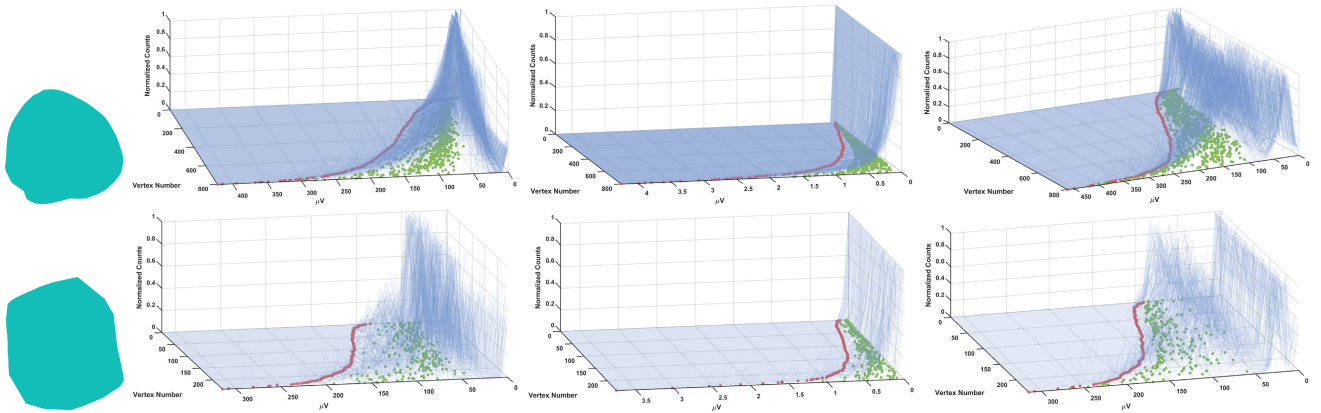
FIGURE 9. TWA maps (left) and histograms of the distribution of TWA in an ICM patient epicardium (top) and torso (bottom), with TWA estimated by the TM (second column), SM (third column), and MMA (right). Red circles denote CI right limits, while green circles represent empirical values for each mesh point, and mesh color indicates conformity of empirical values with their respective CIs.
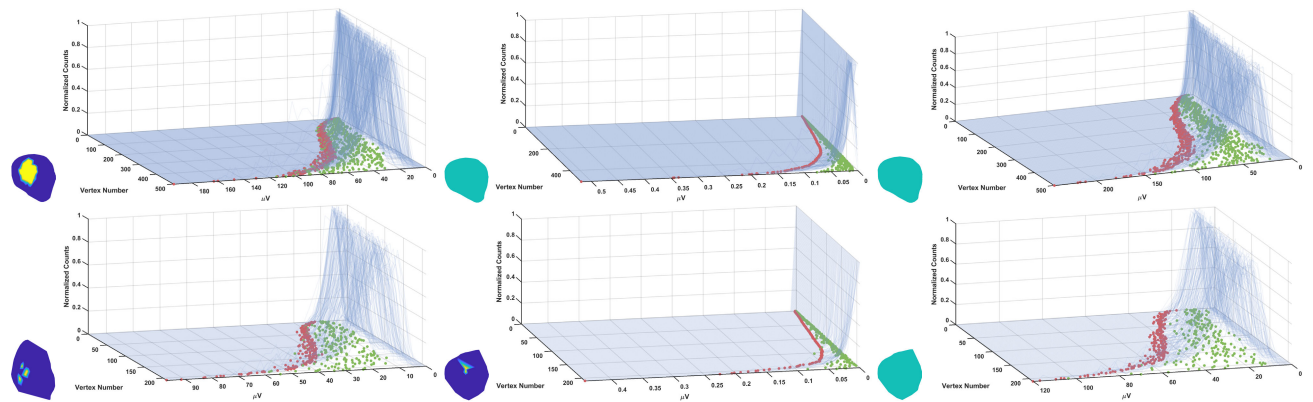

FIGURE 10. Epicardium (top) and torso (bottom) TWA maps (odd columns) and histograms of the distribution of TWA (even columns) in a LQTS patient, with TWA estimated by TM (left), SM (middle), and MMA (right). Red circles denote CI right limits, green circles represent empirical values, and mesh color indicates whether empirical values are inside (blue) or outside (yellow) the CIs, with a blue-green color if all the empirical values are inside their corresponding CI.

idea that the SM is more sensitive and generally performs better.

Analyzing the results provided by the last presented method, it would be convenient to understand how the quantity of both epicardial and torso surfaces detected to be affected by TWA varies as the synthetic alternans amplitude added increases. Synthetic alternans was added to epicardial signals, and torso signals were estimated using the transfer matrix. Since the synthetic alternans was added using a spatial-temporal Gaussian function, the affected epicardium area and the synthetic alternans amplitude are directly related, meaning that as one increases, the other also does. These results are shown in Fig. 7, where we can see that the SM is more sensitive than the TM and the MMA; that is, the area detected as affected is higher in most cases. Additionally, the MMA needs more synthetic alternans amplitude to detect the presence of TWA, which is not always achieved, for instance, in the torso of synthetic subject 1.

Figure 8 illustrates the epicardium and torso of control subject 2 when $125\mu V$ of synthetic alternans amplitude

were added. Even though only results for this patient are shown, equivalent results are obtained for control subject 1 when $325\mu V$ of synthetic alternans amplitude were added. Regarding the epicardium, the area where the alternans were added is well recognized when using the three estimation methods; however, results in the torso are more diffuse. In general, the detected areas do not coincide with the more prominent ones when bootstrap was not employed, although these areas are not free of TWA either. This may be due to the nature of the direct problem of cardiology, which tends to diminish the signal amplitude in the torso, complicating the process of detecting alternans. Nevertheless, it is clear that when TWA is present in the epicardium, it is observable in the torso.

Finally, the method was tested on real patients with illnesses. Figure 9 presents the results for an ICM patient, while Fig. 10 displays the results for a LQTS patient. Torso signals were obtained through body surface potential mapping instead of using the corresponding transfer matrix, as it was unavailable for the LQTS patient. Results are

negative for the ICM patient in both the epicardium and torso using the three estimation methods. However, TWA was detected in an area of the LQTS patient's epicardium when using the TM and in the torso when using the TM and the SM. TWA signals were extracted with traditional methodologies, and results coincided with the area labeled as problematic.

V. DISCUSSION AND ANALYSIS OF RESULTS

The focus of this study was the generation of a reference that allows the precise evaluation of TWA estimation methods, incorporating a novel T-wave segmentation technique specific to ECGI data. Additionally, a statistical approach that ascertains the presence of TWA by determining the significance of differences between consecutive T-waves is presented. Therefore, our main contributions are, first, the quantitative demonstration of the superiority of a novel TWA segmentation method tailored to ECGI previously introduced in [18], second, the creation of the reference as a high-fidelity means to rigorously test emerging TWA estimation methods, and third, the introduction of a novel binary classifier to aid in decisions regarding the presence of TWA. Despite the emergence of numerous studies on TWA estimation in recent years, the novelty of our study lies in generating a reference to facilitate the comparison of different estimation methodologies, with a specific focus on ECGI, and introducing a Bootstrap-based binary classifier to determine the presence or absence of TWA.

A. SUPERIORITY OF THE SRS OVER THE AS

The comparison of the two T-wave segmentation methods reveals that SRS segmentations are of better quality than AS ones, both qualitatively and quantitatively, as depicted in both Fig. 1 and Tab. 2, supporting the idea that the heart functions synchronously. Despite its simplicity, the SRS has proven to be a potential segmentation method for ECGI data, outperforming other approaches. Qualitatively, the subtraction of even and odd T-waves provides a decidedly smoother signal, both in control subjects and patients (see Fig. 1 (a)), as previously advanced in [18]. These results are quantitatively supported by statistical analyses, demonstrating the significantly superior performance of the SRS over the commonly used AS methodology (see Fig. 1 (b) and Tab. 2).

B. ANALYSIS OF THE REFERENCE

Despite the existence of several TWA estimation methods, a definitive gold standard that significantly outperforms other approaches had not been established. Among the various possible reasons for this, the lack of a standardized reference in the literature for testing, comparing, and accurately assessing the performance, strengths, and limitations of these estimation methods stands out. Consequently, we undertook the development of a reference, as realistic as possible, to address these previously outlined limitations. Considerable care was taken in creating the reference and introducing synthetic alternans to maintain a realistic model. The reference

was generated by repeating beats from real subjects rather than synthetically generating ECG signals from scratch. Similarly, the addition of alternans followed a realistic approach since TWA typically presents in cardiac signals with a very small amplitude on the order of microvolts, making it challenging to differentiate from noise. To introduce alternans realistically, a low-amplitude spatial-temporal Gaussian was employed to subtly modify T-waves, facilitating the study of the sensitivity of estimation methods. As stated earlier, alternans are often intertwined with noise, underscoring the priority of proper noise elimination when attempting to estimate TWA. Additionally, it is crucial to prevent applied filters from erasing physiological information; hence, the careful design of filters assumes paramount importance. Our noise analysis, presented in Fig. 3 and performed using the developed reference, highlights the consistency of our filters. Even when noise levels are relatively high, specifically at $175\mu V$ and $200\mu V$ for baseline and white noise amplitudes, respectively, both filters perform correctly, generating residuals with amplitudes significantly smaller than the signal amplitude (Fig. 3 (e) and (f)). Upon examining TWA estimations using the TM, SM, and MMA methods, it is evident that these methods correctly identify the area where synthetic alternans were added when no noise is introduced, as expected (see Fig. 4, first row). This validates the correct generation of the reference and demonstrates the effectiveness of the three evaluated estimation methods, at least in the simplest scenario. However, challenges arise when noise is introduced. For instance, with the addition of $175\mu V$ of baseline noise, the TM and SM provide TWA estimations similar to those without added noise, but MMA estimations become noisier, especially in the torso, where the alternan signal becomes indistinguishable from the noise (see Fig. 4, second row). Regarding white noise, when $200\mu V$ of noise amplitude is added and subsequently filtered, all three methods yield noisier estimations, with MMA estimates being the noisiest (see Fig. 4, third row). The SM appears to be the more consistent method, with stable TWA estimations that remain relatively unchanged even in the presence of noise. Transitioning from controlled situations to real scenarios, adding approximately $55\mu V$ of synthetic alternans amplitude to real control subjects is sufficient to distinguish TWA from noise using the estimation methods (see Fig. 5). This analysis highlights the stable behavior of the SM, which behaves similarly in the two control subjects, unlike the other methods, with MMA proving to be more affected by noise.

C. BOOTSTRAP APPROACH FOR TWA DETECTION

The application of statistical methods for determining the presence of a disease instills positivity and confidence in the diagnostic process. While observing alternan signals provides insights into the potential presence of TWA, there lacks a direct method for unequivocally identifying TWA. In response, we have developed a bootstrap-based method for identifying areas exhibiting TWA, demonstrating a consistent

performance. In real control subjects where no TWA has been added, the method appropriately detects the absence of TWA, aligning with expectations (see Fig. 6). Upon introducing synthetic alternans, the method begins detecting TWA in the epicardium when the alternans amplitude approaches approximately $50\mu V$ (see Fig. 7). This consistency aligns with previously obtained results, albeit subject-dependent. Conversely, in the torso, a higher epicardium area needs to be affected for the method to recognize TWA presence. Upon introducing sufficient synthetic alternans for TWA detection in the torso, the method accurately identifies the epicardium area when employing the TM, SM, and MMA bootstrap approaches. However, in the torso, a specific area is identified (see Fig. 8), with the MMA-based result appearing more uncertain across different patients. According to these results, one limitation could be that the method may under-recognize the presence of TWA, especially when the affected area in the heart is small. Results from patients corroborate our expectations. Figure 9 illustrates that the ICM patient does not exhibit TWA, with all methods reaching the same conclusion. In contrast, the LQT patient in Fig. 10 displays a sizable area in the epicardium with TWA, particularly evident when using the TM. In the torso, where signals are obtained through body surface potential mapping rather than estimations, specific small areas suggest the potential presence of alternans. In both the epicardium and torso areas, alternan signals derived from the estimation methods appear to indicate the presence of TWA.

D. FINAL REMARKS AND FUTURE DIRECTIONS

Neither ECGI nor TWA estimation are currently incorporated into clinical practice, and ECGI algorithms are still being improved to yield clinically relevant results. Whereas standard ECG studies are unable to precisely identify where electrical events occur in the heart, ECGI provides information in both the temporal and spatial domains, offering an anatomical view to address this limitation. Although the distribution of alternans throughout the heart is currently unknown, ECGI and the anatomical view it provides could shed light on it and help elucidate their mechanisms. In light of this, ECGI can improve TWA detection, justifying the steps taken in this direction. In previous years, there was a lack of tools to determine the presence of TWA. The emergence of tools for hypothesis or decision tests, like the one presented in this work, solves this problem by taking advantage of the anatomical map provided by ECGI. Our contribution here is not only the generation of a binary classifier, but we have also found that optimal cutoff values for TWA detection are patient dependent, an important consideration for our future studies. More work remains, but these statistical methods could play a relevant role in implementing TWA estimation methods in clinical practice. It is fundamental to consolidate TWA estimation methods using ECGI before including them in clinical practice. This study paves the way towards adopting a more clinical point of view of ECGI in TWA and pathological scenarios like LQTS.

VI. CONCLUSION

In this work, the three previously enumerated objectives have been successfully addressed and achieved. Objective (i) involved quantitatively demonstrating that the SRS outperforms commonly used methods in segmenting T-waves in ECGI data. This was successfully demonstrated due to the intrinsic nature of the SRS, which is the first T-wave segmentation procedure specifically tailored to ECGI data. Objective (ii) involved designing and developing a reference that can serve as a gold standard for analyzing the performance of estimation methods, helping to determine the most accurate TWA estimation method. Finally, objective (iii) involved the development of a Bootstrap-based TWA detector, which appears to recognize the areas with TWA. This demonstrated that a non-parametric test intrinsic to each subject helps identify the areas of the epicardium and torso where TWA is more prominent. The positive results obtained open new doors and necessitate further study. In the future, we could explore alternative TWA estimation methods beyond traditional ones and use the presented reference for comparison purposes. It would also be interesting to refine and strengthen the presented Bootstrapping technique to improve its consistency and rigor, making it a potential tool for clinical use in the future.

REFERENCES

[1] M. J. Cutler and D. S. Rosenbaum, "Explaining the clinical manifestations of T wave alternans in patients at risk for sudden cardiac death," *Heart Rhythm*, vol. 6, no. 3, pp. S22–S28, Mar. 2009.

[2] A. A. Armoundas, G. F. Tomaselli, and H. D. Esperer, "Pathophysiological basis and clinical application of T-wave alternans," *J. Amer. College Cardiol.*, vol. 40, pp. 207–217, Jul. 2002.

[3] F. J. Gimeno-Blanes, M. Blanco-Velasco, Ó. Barquero-Pérez, A. García-Alberola, and J. L. Rojo-Álvarez, "Sudden cardiac risk stratification with electrocardiographic indices—A review on computational processing, technology transfer, and scientific evidence," *Frontiers Physiol.*, vol. 7, no. 82, pp. 1–17, Mar. 2016.

[4] S. M. Narayan, "T-wave alternans and the susceptibility to ventricular arrhythmias," *J. Amer. College Cardiol.*, vol. 47, no. 2, pp. 269–281, Jan. 2006.

[5] D. S. Rosenbaum, P. Albrecht, and R. J. Cohen, "Predicting sudden cardiac death from T wave alternans of the surface electrocardiogram: Promise and pitfalls," *J. Cardiovascular Electrophysiol.*, vol. 7, no. 11, pp. 1095–1111, Nov. 1996.

[6] T. Nieminen and R. L. Verrier, "Usefulness of T-wave alternans in sudden death risk stratification and guiding medical therapy," *Ann. Noninvasive Electrocardiol.*, vol. 15, pp. 276–288, Jul. 2010.

[7] T. You, C. Luo, K. Zhang, and H. Zhang, "Electrophysiological mechanisms underlying T-wave alternans and their role in arrhythmogenesis," *Frontiers Physiol.*, vol. 12, no. 614946, pp. 1–17, Mar. 2021.

[8] Y. Yang, T. Lv, S. Li, and P. Zhang, "The relationship between T-wave alternans and adverse cardiac events in patients with congenital long QT syndrome: A systematic review and meta-analysis," *Congenital Heart Disease*, vol. 17, no. 5, pp. 557–567, Jun. 2022.

[9] J. A. Kannampuzha, P. Sengodan, S. Avula, B. White, S. J. Ganocy, P. J. Leo, and E. S. Kaufman, "Non-sustained microvolt level T-wave alternans in congenital long QT syndrome types 1 and 2," *J. Electrocardiol.*, vol. 51, no. 2, pp. 303–308, Mar./Apr. 2018, doi: 10.1016/j.jelectrocard.2017.11.008.

[10] R. Caulier-Cisterna, M. Sanromán-Junquera, S. Muñoz-Romero, M. Blanco-Velasco, R. Goya-Esteban, A. García-Alberola, and J. L. Rojo-Álvarez, "Spatial–temporal signals and clinical indices in electrocardiographic imaging (I): Preprocessing and bipolar potentials," *Sensors*, vol. 20, no. 11, pp. 1–28, Jun. 2020, Art. no. 3131.

[11] N. G. Kavesh, S. R. Shorofsky, S. E. Sarang, and M. R. Gold, "Effect of heart rate on T wave alternans," *J. Cardiovascular Electrophysiology*, vol. 9, no. 7, pp. 703–708, Jul. 1998.

[12] J. Lewek, P. Ptaszynski, T. Klingenheben, and I. Cygankiewicz, "The clinical value of T-wave alternans derived from Holter monitoring," *Eur. Heart J. Arrhythmias Electrophysiol.*, vol. 19, pp. 529–534, Apr. 2017.

[13] R. Caulier-Cisterna, M. Blanco-Velasco, R. Goya-Esteban, S. Muñoz-Romero, M. Sanromán-Junquera, A. García-Alberola, and J. L. Rojo-Álvarez, "Spatial–temporal signals and clinical indices in electrocardiographic imaging (II): Electrogram clustering and T-wave alternans," *Sensors*, vol. 20, no. 11, p. 3070, May 2020.

[14] C. Ramanathan, R. N. Ghanem, P. Jia, K. Ryu, and Y. Rudy, "Noninvasive electrocardiographic imaging for cardiac electrophysiology and arrhythmia," *Nature Med.*, vol. 10, no. 4, pp. 422–428, Apr. 2004.

[15] H. S. Oster, B. Taccardi, R. L. Lux, P. R. Ershler, and Y. Rudy, "Noninvasive electrocardiographic imaging: Reconstruction of epicardial potentials, electrograms, and isochrones and localization of single and multiple electrocardiac events," *Circulation*, vol. 96, no. 3, pp. 1012–1024, Aug. 1997.

[16] Y. Rudy, "Noninvasive ECG imaging (ECGI): Mapping the arrhythmic substrate of the human heart," *Int. J. Cardiology*, vol. 237, pp. 13–14, Jun. 2017.

[17] Y. Wang, P. S. Cuculich, J. Zhang, K. A. Desouza, R. Vijayakumar, J. Chen, M. N. Faddis, B. D. Lindsay, T. W. Smith, and Y. Rudy, "Noninvasive electroanatomic mapping of human ventricular arrhythmias with electrocardiographic imaging," *Sci. Transl. Med.*, vol. 3, no. 98ra84, pp. 1–22, Aug. 2011.

[18] E. Sánchez-Carballo, F.-M. Melgarejo-Meseguer, J. L. Rojo-Alvarez, A. García-Alberola, and Y. Rudy, "Single reference segmentation to estimate T-wave alternans," in *Proc. Comput. Cardiol. Conf. (CinC)*, Atlanta, GA, USA, Nov. 2023, pp. 1–4.

[19] S. Richter, G. Duray, and S. H. Hohnloser, "How to analyze T-wave alternans," *Heart Rhythm*, vol. 2, no. 11, pp. 1268–1271, Nov. 2005.

[20] M. Yuan, H. Lian, and P. Li, "Spatiotemporal patterns of early afterdepolarizations underlying abnormal T-wave morphologies in a tissue model of the purkinje-ventricular system," *PLoS ONE*, vol. 18, no. 1, pp. 1–13, Jan. 2023, Art. no. e0280267.

[21] T. You, Y. Xie, C. Luo, K. Zhang, and H. Zhang, "Mechanistic insights into spontaneous transition from cellular alternans to ventricular fibrillation," *Physiol. Rep.*, vol. 11, no. 5, pp. 1–21, Mar. 2023.

[22] J. L. Rojo-Álvarez, R. Goya-Esteban, S. Muñoz-Romero, A. García-Alberola, F. M. Melgarejo-Meseguer, and M. Blanco-Velasco, "T-wave alternans analysis with electrocardiographic imaging," in *Proc. Comput. Cardiol. Conf. (CinC)*, Maastricht, The Netherlands, Jun. 2019, pp. 1–4.

[23] L. R. Bear, M. Cluitmans, E. Abell, J. Rogier, L. Labrousse, L. K. Cheng, I. LeGrice, N. Lever, G. B. Sands, B. Smaill, M. Haïssaguerre, O. Bernus, R. Coronel, and R. Dubois, "Electrocardiographic imaging of repolarization abnormalities," *J. Amer. Heart Assoc.*, vol. 10, no. 9, pp. 1–12, May 2021.

[24] L. D. Palma, V. I. D'Alessandro, F. Attivissimo, A. D. Nisio, and A. M. L. Lanzolla, "ECG wave segmentation algorithm for complete P-QRS-T detection," in *Proc. IEEE Int. Symp. Med. Meas. Appl. (MeMeA)*, Jun. 2023, pp. 1–6.

[25] A. Darmawahyuni, S. Nurmaini, M. N. Rachmatullah, P. P. Avi, S. B. P. Teguh, A. I. Sapitri, B. Tutuko, and F. Firdaus, "Improved delineation model of a standard 12-lead electrocardiogram based on a deep learning algorithm," *BMC Med. Informat. Decis. Making*, vol. 23, no. 1, pp. 1–15, Jul. 2023.

[26] W. Wang, H. Ni, and H. Zhang, "Investigation of the mechanisms underlying cardiac alternans–insights from a computational study," in *Proc. Comput. Cardiol. Conf. (CinC)*, Nice, France, Sep. 2015, pp. 1101–1104.

[27] B. D. Nearing and R. L. Verrier, "Novel application of convolutional neural networks for artificial intelligence-enabled modified moving average analysis of P-, R-, and T-wave alternans for detection of risk for atrial and ventricular arrhythmias," *J. Electrocardiol.*, vol. 83, pp. 12–20, Mar. 2024.

[28] T. Winkert, J. Nadal, and P. R. Benchimol-Barbosa, "Baseline drifting correction for automated MTWA measurements," in *Proc. Comput. Cardiol. Conf. (CinC)*, Atlanta, GA, USA, Nov. 2023, pp. 1–4.

[29] T. A. A. Abdullah, M. S. M. Zahid, W. Ali, and S. U. Hassan, "B-LIME: An improvement of LIME for interpretable deep learning classification of cardiac arrhythmia from ECG signals," *Processes*, vol. 11, no. 2, pp. 1–19, Feb. 2023, Art. no. 595.

[30] A. McWilliam, A. Abravan, K. Banfill, C. Faivre-Finn, and M. van Herk, "Demystifying the results of RTOG 0617: Identification of dose sensitive cardiac subregions associated with overall survival," *J. Thoracic Oncol.*, vol. 18, no. 5, pp. 599–607, May 2023.

[31] B. D. Nearing and R. L. Verrier, "Modified moving average analysis of T-wave alternans to predict ventricular fibrillation with high accuracy," *J. Appl. Physiol.*, vol. 92, no. 2, pp. 541–549, Feb. 2002.

[32] R. Vijayakumar, J. N. A. Silva, K. A. Desouza, R. L. Abraham, M. Strom, F. Sacher, G. F. Van Hare, M. Haïssaguerre, D. M. Roden, and Y. Rudy, "Electrophysiologic substrate in congenital long QT syndrome: Noninvasive mapping with electrocardiographic imaging (ECGI)," *Circulation*, vol. 130, no. 22, pp. 1936–1943, Nov. 2014.

[33] P. S. Cuculich, J. Zhang, Y. Wang, K. A. Desouza, R. Vijayakumar, P. K. Woodard, and Y. Rudy, "The electrophysiological cardiac ventricular substrate in patients after myocardial infarction: Noninvasive characterization with electrocardiographic imaging," *J. Amer. College Cardiol.*, vol. 58, no. 18, pp. 1893–1902, Oct. 2011.

ESTELA SÁNCHEZ-CARBALLO received the bachelor's degree in biomedical engineering from Universidad Rey Juan Carlos, Madrid, Spain, in 2022, and the master's degree in information health engineering from Universidad Carlos III de Madrid, in 2023. She is currently pursuing the Ph.D. degree with Universidad Rey Juan Carlos. In 2022, she was with the Department of Signal Theory and Communications, Universidad Rey Juan Carlos, as a Research Assistant. Her research interests include statistical learning methods for signal and image processing, arrhythmia mechanisms, robust signal processing techniques, inverse problems in cardiology sensors, and data science for healthcare.

FRANCISCO MANUEL MELGAREJO-MESEGUER received the bachelor's and master's degrees in telecommunication engineering from the Miguel Hernández University of Elche, Spain, in 2014 and 2016, respectively, and the Ph.D. degree in multimedia and communications from Universidad Rey Juan Carlos, Madrid, in 2019. From 2015 to 2019, he was a Predoctoral Fellow at Hospital Clínico Universitario Virgen de la Arrixaca, Murcia. In 2019, he was an Assistant Professor with the University of Murcia. Since 2020, he has been an Associate Professor with Universidad Rey Juan Carlos, specifically with the Department of Signal Theory and Communications, specializing in bio-signal processing, deep learning, and machine learning, with over 15 publications and 100 citations. His research interests include statistical learning methods for signal and image processing, studying arrhythmia mechanisms, developing robust signal processing techniques, addressing inverse problems in cardiology sensors, and applying data science to biological signal processing.

RAMYA VIJAYAKUMAR received the B.Sc. degree in computer engineering from the University of Ottawa, Canada, in 2003, the M.S. degree in biomedical engineering from Rutgers University, The State University of New Jersey, in 2007, and the Ph.D. degree in biomedical engineering from Washington University in St. Louis, St. Louis, MO, USA, in 2016. She is currently a Scientist with the Department of Surgery, Washington University School of Medicine. Her research interests include electrophysiologic substrate and arrhythmia mechanisms in mitral regurgitation patients using noninvasive electrocardiographic imaging.

JUAN JOSÉ SÁNCHEZ-MUÑOZ received the M.D. and Ph.D. degrees from Universidad de Murcia, Spain, in 1987 and 2000, respectively. Since 1995, he has been a Cardiac Electrophysiologist with the Hospital Clínico Universitario Virgen de la Arrixaca and an Assistant Professor of medicine with Universidad de Murcia, where he is currently a Consultant Cardiologist with the Arrhythmia Unit of Cardiac Electrophysiology. He has co-authored more than 40 scientific articles and more than 50 communications in cardiac electrophysiology. His research interests include arrhythmia mechanisms and cardiac signal processing in ventricular fibrillation.

ARCADI GARCÍA-ALBEROLA received the M.D. and Ph.D. degrees from Universitat de Valencia, Burjassot, Spain, in 1982 and 1991, respectively. Since 1993, he has been a Cardiologist and a Professor of medicine with the Hospital Clínico Universitario Virgen de la Arrixaca and Universidad de Murcia, Murcia, Spain, where he is currently the Director of the Arrhythmia Unit of Cardiac Electrophysiology. He has co-authored more than 130 scientific articles and more than 60 communications in cardiac electrophysiology. His research interests include repolarization analysis, arrhythmia mechanisms, and cardiac signal processing.

YORAM RUDY received the B.Sc. and M.Sc. degrees from the Technion—Israel Institute of Technology, in 1970 and 1973, respectively, and the Ph.D. degree from Case Western Reserve University, in 1978, where he also attended the first two years of medical school. In 1994, he established the interdisciplinary Cardiac Bioelectricity Research and Training Center and became the Director. He was also a Visiting Professor at various universities worldwide. He is currently a Distinguished Professor Emeritus at Washington University in St. Louis, where he established and directed the Cardiac Bioelectricity and Arrhythmia Center. He has published over 300 scientific articles and graduated 30 Ph.D. students. He is a member of the National Academy of Engineering and Fellow of the National Academy of Inventors. He was a recipient of numerous awards, including the NIH Merit Award, the Biomedical Engineering Society Distinguished Lectureship Award, the Heart Rhythm Society Distinguished Scientist Award, the Case Western Reserve University Distinguished Alumni Award, and the Hein Wellens Distinguished Professor in Cardiology at Maastricht University. He also served as the President for the Cardiac Electrophysiology Society.

JOSÉ LUIS ROJO-ÁLVAREZ (Senior Member, IEEE) received the B.Sc. degree in telecommunication engineering from Universidade de Vigo, in 1996, and the Ph.D. degree in telecommunication engineering from Universidad Politécnica de Madrid, in 2000. He is currently a Full Professor with the Department of Signal Theory and Communications, Universidad Rey Juan Carlos, Spain. He has co-authored more than 160 international articles and contributed to more than 180 conference proceedings. His research interests include statistical learning methods for signal and image processing, arrhythmia mechanisms, robust signal processing techniques, inverse problems in cardiology sensors, and data science for healthcare.

• • •